Journal of Sound and Vibration (1999) **221**(3), 351–369
Article No. jsvi.1998.1985, available online at http://www.idealibrary.com on IDEAL

ACTIVE CONTROL OF RADIATED DUCT NOISE WITH AN INSUFFICIENT NUMBER OF SENSORS AND ACTUATORS

D.-B. YOON AND Y.-H. KIM

Center for Noise and Vibration Control, Department of Mechanical Engineering, Korea Advanced Institute of Science and Technology, Science Town, Taejon 305-701, *Korea*

(*Received* 11 *November* 1997, *and in final form* 14 *September* 1998)

If one wants to control the noise from a duct, then one must have a sufficient number of sensors and actuators so that the control system is observable and controllable. The number of sensors and actuators for controlling radiating noise from a duct has to be incorporated with the number of modes that one wants to control. These considerations motivated the present study which considers a control system that has fewer sensors and actuators than the number of propagating modes in a duct. The control performance and robust reliability of such a kind of control system are investigated, theoretically and numerically. The likelihood of success in reducing the radiation power of a duct is verified by theoretical analysis and numerical simulations. In addition, the control performance of the control system is verified by experiments.

1. INTRODUCTION

When the lateral dimension of a duct is larger than or comparable to the wavelengths of interest, the higher order modes propagate in the duct. These modes will be radiated, depending on their radiation efficiencies, and produce noise in the exterior region.

If one wants to apply an active noise control method for this case, one has to have the necessary number of sensors and actuators. The sensors must be located where the observability of the control system is guaranteed. The actuators have to be located where its controllability will be satisfied. Typical examples of this kind can be found in references [1, 2]. In these studies, the first four propagating modes in a square duct have been controlled using four sensors and actuators corresponding to the number of propagating modes.

Figure 1 is a schematic diagram that illustrates the relations between sound field variables, control system variables, and residual radiation power at duct termination.

If one has fewer sensors and actuators than required for its controllability and observability, then one may not achieve the desired noise reduction. This can be

0022–460X/99/130351 + 19 $30.00/0

interpreted in a different manner where one could have "some" noise reduction even if one does not have a sufficient number of sensors and actuators. Our first objective is to examine the possibility of obtaining noise reduction when we have fewer sensors and actuators than the number of propagating modes in a duct.

This situation could happen in many practical cases. For example, for fairly large ducts, it is easy to have more than three modes involved in radiating noise. What if one uses only one sensor and one actuator in this case? Is there any chance of achieving noise reduction?

The problem is to find a control strategy for the duct, whose number of propagating modes is known, but whose modal participation is unknown, by using a smaller number of sensors and actuators than the number of propagating modes in a duct. The locations of sensors and actuators are the variables one can use.

The first thing to do will be a mathematical formulation associated with the problem. In section 2, the equations of residual radiation power, which is a global measure of the resulting noise, will be derived as a function of sound field variables and control system variables. In sections 3 and 4, the control performance and robust reliability [3] of the control system will be investigated in terms of sound field variables and control system variables. In addition, the possibility of implementing the robust radiation power control system will be investigated. In section 5, numerical simulation and experiments will be performed to confirm the theoretical results obtained in sections 3 and 4.

2. RESIDUAL RADIATION POWER

As the first step, the equations of residual radiation power, after control, will be derived as a function of sound field variables and control system variables. The unknown pressure field at duct termination due to arbitrary primary sources will be considered as sound field variables. The number and location of control sources and sensors will be considered as control system variables.

2.1. PRESSURE FIELD DUE TO PRIMARY AND CONTROL SOURCES

Let $p^p(r, \theta, 0)$ represent acoustic pressure at the open end of a hard-walled circular duct due to arbitrary primary sources (Figure 2). Then, $p^p(r, \theta, 0)$ can be

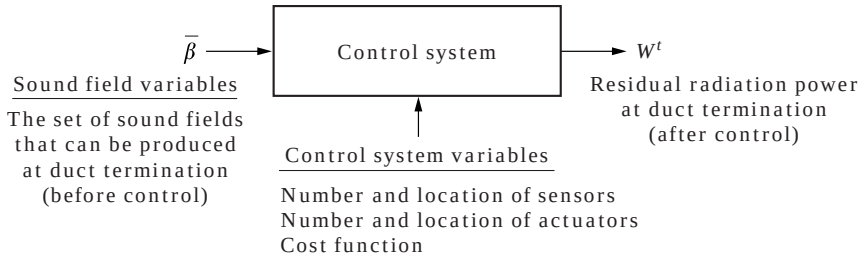

Figure 1. The relations between sound field variables, control system variables, and residual radiation power at duct termination.

$$W^p = \int_A \frac{1}{2} \mathrm{Re}\{p^p(r, \theta, 0)^* \, \mathbf{u}^p(r, \theta, 0)\} \cdot \mathbf{n}_A \, dA$$

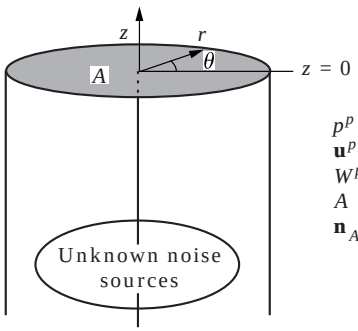

$p^p(r,\theta,0)$: pressure at duct termination ($z=0$)
$\mathbf{u}^p(r,\theta,0)$: particle velocity at duct termination
W^p : radiation power due to primary sources
A : duct area
$\mathbf{n}_A$: unit normal vector of A

Figure 2. The noise emitted from a duct and its acoustic radiation power (W^p).

expressed in terms of the eigenfunctions of the duct's cross-section ($\psi_n(r, \theta)$), and its modal pressure amplitudes (β_n) as

$$p^p(r, \theta, 0) = \sum_{n=1}^{N} \beta_n \psi_n(r, \theta), \tag{1}$$

where N is the number of the propagating modes in the duct, which can be determined if the radius of the duct (r_o) and the frequency range of the primary sources are known [4] (Table 1).

In a matrix form, $p^p(r, \theta, 0)$ can be rewritten as an inner product of $\overline{\psi}$ and $\overline{\beta}$.

$$p^p(r, \theta, 0) = \overline{\psi}\overline{\beta}, \tag{2}$$

where $\overline{\psi} = \{\psi_1(r, \theta), \psi_2(r, \theta), \ldots, \psi_N(r, \theta)\}$ is the $(1 \times N)$ matrix of the eigenfunctions of a duct cross-section, and $\overline{\beta} = \{\beta_1, \beta_2, \ldots, \beta_N\}^T$ is the $(N \times 1)$ matrix whose amplitudes are variables.

Let $p^c(r, \theta, 0)$ denote the pressure at duct termination due to K control sources located at $\mathbf{x}_k^c = (r_k^c, \theta_k^c, z^c)$ (Figure 3). Then, $p^c(r, \theta, 0)$ can be expressed as [5–7]

$$p^c(r, \theta, 0) = \sum_{n=1}^{N} \left(\psi_n(r, \theta) \sum_{k=1}^{K} \left(\frac{\rho\omega}{2Ak_{zn}} (1 + R_n) \, e^{jk_{zn}z^c} \psi_n(r_k^c, \theta_k^c)^* q_k \right) \right), \tag{3}$$

TABLE 1

Eigenfunctions of duct's cross-section ($\psi_n(r, \theta)$) and wave number in r direction (k_{rn})

n	1	2	3
k_{rn}	0	$1{\cdot}84/r_0$	$1{\cdot}84/r_0$
$\psi_n(r, \theta)$	○	⊕	⊖
	1	$N_2 J_1(k_{r2} r) \cos\theta$	$N_3 J_1(k_{r3} r) \sin\theta$
$f_{cut\text{-}off}$	0 Hz	419 Hz	419 Hz

r_0: radius of duct (0·24 m).
N_2, N_3: normalization factor of eigenfunction ($N_2 = N_3 = 2{\cdot}8954$).

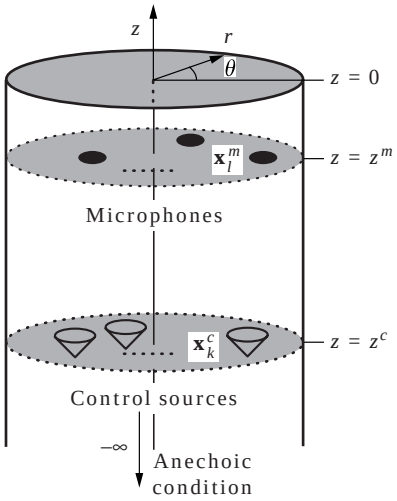

Figure 3. Schematic diagram of the active control system with K control sources and L error microphones.

where ρ is the density of air, ω is the frequency, A is the duct cross-sectional area, k_{zn} is the wave number in z direction, and R_n is the pressure reflection coefficient at duct termination [7]. The superscript "*" denotes complex conjugate, and q_k is the volume velocity of the kth control source. In a matrix form, $p^c(r, \theta, 0)$ can be expressed as equation (4a) in terms of $\bar{q}$, $\mathbf{\Psi}^c$, and $\mathbf{T}^c$.

$$p^c(r, \theta, 0) = \bar{\psi}\mathbf{T}^c\mathbf{\Psi}^c\bar{q}, \tag{4a}$$

$$\bar{q} = \{q_1, q_2, \ldots, q_K\}^T, \tag{4b}$$

$$\mathbf{\Psi}^c = \begin{bmatrix} \psi_1(r_1^c, \theta_1^c)^* & \cdots & \psi_1(r_K^c, \theta_K^c)^* \\ \vdots & \ddots & \vdots \\ \psi_N(r_1^c, \theta_1^c)^* & \cdots & \psi_N(r_K^c, \theta_K^c)^* \end{bmatrix}, \tag{4c}$$

$$\mathbf{T}^c = \begin{bmatrix} T_{11}^c & \cdots & 0 \\ \vdots & \ddots & \vdots \\ 0 & \cdots & T_{NN}^c \end{bmatrix}, \quad T_{nn}^c = \frac{\rho\omega}{2Ak_{zn}}(1 + R_n)\, e^{ik_{zn}z^c}. \tag{4d, e}$$

Let $p^t(r, \theta, 0)$ represent the pressure at duct termination due to primary and control sources. Then, from equations (2) and (4a), $p^t(r, \theta, 0)$ can be expressed as

$$p^t(r, \theta, 0) = \bar{\psi}(\bar{\beta} + \mathbf{T}^c\mathbf{\Psi}^c\bar{q}), \tag{5}$$

where $\bar{\beta}$ and $\mathbf{T}^c\mathbf{\Psi}^c\bar{q}$ represent the modal pressure amplitudes due to primary and control sources, respectively.

2.2. COST FUNCTION AND RESIDUAL PRESSURE FIELD

Various cost functions, for example, acoustic potential energy, acoustic energy density, sound intensity, etc., can be used for the reduction of duct noise. Among these cost functions, the acoustic potential energy is the simplest one to measure. The cost function employed in this study is the acoustic potential energy at the error microphone locations.

Let $\bar{p}^m$ be the measured pressure vector of $(L \times 1)$ at the error microphones which are located at $\mathbf{x}_l^m = (r_l^m, \theta_l^m, z^m)$ (Figure 3). Then, $\bar{p}^m$ can be expressed as equation (6a) in terms of $\mathbf{\Psi}^m$ and $\mathbf{T}^m$.

$$\bar{p}^m = \mathbf{\Psi}^{m\prime}\mathbf{T}^m(\overline{\beta} + \mathbf{T}^c\mathbf{\Psi}^c\bar{q}), \tag{6a}$$

$$\mathbf{\Psi}^m = \begin{bmatrix} \psi_1(r_1^m, \theta_1^m) & \cdots & \psi_N(r_1^m, \theta_1^m) \\ \vdots & \ddots & \vdots \\ \psi_1(r_L^m, \theta_L^m) & \cdots & \psi_N(r_L^m, \theta_L^m) \end{bmatrix}, \tag{6b}$$

$$\mathbf{T}^m = \begin{bmatrix} T_{11}^m & \cdots & 0 \\ \vdots & \ddots & \vdots \\ 0 & \cdots & T_{NN}^m \end{bmatrix}, \quad T_{nn}^m = \frac{1}{1+R_n}\,\mathrm{e}^{-jk_{zn}z^m} + \frac{R_n}{1+R_n}\,\mathrm{e}^{jk_{zn}z^m}. \tag{6c, d}$$

Then, the cost function (J), which represents the acoustic potential energy at the error microphone locations, can be expressed as

$$J = \bar{p}^{m^H}\bar{p}^m. \tag{7}$$

where the superscript "H" denotes Hermitian transpose.

Some manipulations lead to the following expression for $\bar{q}$ which minimize J.

$$\bar{q} = -(\mathbf{\Psi}^{m\prime}\mathbf{T}^{m\prime}\mathbf{T}^c\mathbf{\Psi}^c)^+\mathbf{\Psi}^{m\prime}\mathbf{T}^m\overline{\beta}, \tag{8}$$

where superscript "$+$" implies the Moore–Penrose generalized matrix inverse [8].

Substitution of equation (8) into equation (5) yields

$$p^t(r, \theta, 0) = \overline{\psi}(\mathbf{I} - \mathbf{T}^c\mathbf{\Psi}^c(\mathbf{\Psi}^{m\prime}\mathbf{T}^{m\prime}\mathbf{T}^c\mathbf{\Psi}^c)^+\mathbf{\Psi}^{m\prime}\mathbf{T}^m)\overline{\beta}, \tag{9}$$

where $\mathbf{I}$ is the $(N \times N)$ identity matrix.

For convenience, let the second term in the parenthesis of equation (9) be $\mathbf{C}$, that is

$$\mathbf{C} = \mathbf{T}^c\mathbf{\Psi}^c(\mathbf{\Psi}^{m\prime}\mathbf{T}^{m\prime}\mathbf{T}^c\mathbf{\Psi}^c)^+\mathbf{\Psi}^{m\prime}\mathbf{T}^m. \tag{10}$$

Then, the residual pressure field, when J is minimized, can be expressed as a function of the sound field variables and control system variables as

$$p^t(r, \theta, 0) = \overline{\psi}(\mathbf{I} - \mathbf{C})\overline{\beta}. \tag{11}$$

2.3. RESIDUAL RADIATION POWER OF THE DUCT

The residual radiation power, which is a global measure of the resulting noise, can be defined as

$$W^t = \int_A \frac{1}{2} \operatorname{Re} \{p^t(r, \theta, 0)^* \mathbf{u}^t(r, \theta, 0)\} \cdot \mathbf{n}_A \, \mathrm{d}A, \tag{12}$$

where $\mathbf{u}^t(r, \theta, 0)$ is the particle velocity at $z = 0$, and A and $\mathbf{n}_A$ represent the duct cross-sectional area and its unit normal vector respectively.

Substitution of equation (11) into equation (12), and some mathematical rearrangements yield

$$W^t = \int_A [\overline{\psi}(\mathbf{I} - \mathbf{C})\overline{\beta}]^H [\overline{\psi}\mathbf{A}(\mathbf{I} - \mathbf{C})\overline{\beta}] \, \mathrm{d}A, \tag{13}$$

where $\mathbf{A}$ is the $(N \times N)$ diagonal matrix, which consists of the radiation impedance Z_n [7] at duct termination.

$$\mathbf{A} = \begin{bmatrix} A_{11} & \cdots & 0 \\ \vdots & \ddots & \vdots \\ 0 & \cdots & A_{NN} \end{bmatrix}, \quad A_{nn} = \operatorname{Re}\left\{\frac{1}{2Z_n}\right\}. \tag{14}$$

Since the eigenfunctions (Table 1) satisfy the orthonormal condition ($\int_A \overline{\Psi}^H \overline{\psi} \, \mathrm{d}A = \mathbf{I}$), equation (13) can be written in a more compact form, that is

$$W^t = \overline{\beta}^H (\mathbf{I} - \mathbf{C})^H \mathbf{A}(\mathbf{I} - \mathbf{C})\overline{\beta}. \tag{15}$$

In equation (15), one can see that W^t can be expressed as a function of the sound field variable ($\overline{\beta}$) and matrix $\mathbf{C}$ which consists of the control system variables. It is noteworthy that if $\mathbf{C}$ is the $(N \times N)$ identity matrix [1, 2], then W^t vanishes for any value of $\overline{\beta}$.

The aim of this study is to investigate the control performance and robust reliability [3] of a control system which consists of fewer sensors and control sources than the number of propagating modes in a duct. Thus, the control performance and robust reliability of such a control system will be investigated in the following sections.

3. CONTROL PERFORMANCE OF THE CONTROL SYSTEM

In this section, the characteristics of matrix **C**, which is a function of the control system variables, will be investigated. Then, the control performance of the control system will be discussed.

3.1. CHARACTERISTICS OF MATRIX **C**

Since **C** is the $(N \times N)$ matrix, it has N eigenvalues (μ_n) and corresponding eigenvectors $(\bar{u}_n)$ satisfying the relation.

$$\mathbf{C}\bar{u}_n = \mu_n \bar{u}_n, \qquad (n = 1 \sim N). \tag{16}$$

Let the rank of **C** be R, then **C** has R non-zero eigenvalues and $N - R$ zero eigenvalues. If one has one control source $(K = 1)$ and one error microphone $(L = 1)$, then the rank of **C** is 1, and **C** has one non-zero eigenvalue (μ_1) and $N - 1$ zero eigenvalues $(\mu_2 \sim \mu_N)$. This case will be kept in the later part of this section because of its simplicity.

The non-zero eigenvalue and corresponding eigenvector can be found by multiplying equation (10) by $\mathbf{T}^c\mathbf{\Psi}^c$ as

$$\mathbf{C}\mathbf{T}^c\mathbf{\Psi}^c = \mathbf{T}^c\mathbf{\Psi}^c. \tag{17}$$

By comparing equation (17) with equation (16), one can see that the non-zero eigenvalue of **C**, μ_1, is 1 and the corresponding eigenvector, $\bar{u}_1$, is $\mathbf{T}^c\mathbf{\Psi}^c$. It is noteworthy that the location of the control source determines the $\bar{u}_1$.

Since μ_n $(n = 2 \sim N)$ of matrix **C** is zero, the following relation can be easily derived from equation (16).

$$\mathbf{C}\bar{u}_n = \bar{\mathbf{0}}, \qquad (n = 2 \sim N). \tag{18}$$

From equations (10) and (18), one can see that $\bar{u}_2 \sim \bar{u}_N$ satisfies the following orthogonal condition. That is, $(\mathbf{\Psi}^m\mathbf{T}^m)\bar{u}_n = 0$ $(n = 2 \sim N)$. It is noteworthy that $(\mathbf{\Psi}^m\mathbf{T}^m)^H$ represents the vector that is orthogonal to $\bar{u}_2 \sim \bar{u}_N$. Table 2 summarizes the eigenvalues (μ_n) and eigenvectors $(\bar{u}_n)$ of matrix **C**.

3.2. CONTROL PERFORMANCE OF THE CONTROL SYSTEM

The sound field variable $(\bar{\beta})$ can be expressed as a function of $\bar{u}_n$ $(n = 1 \sim N)$, such as

$$\bar{\beta} = \sum_{n=1}^{N} c_n \bar{u}_n. \tag{19}$$

TABLE 2

Eigenvalues (μ_n) *and eigenvectors* $(\bar{u}_n)$ *of matrix* **C** $(K = L = 1)$

n	1	$2 \sim N$
μ_n	1	0
$\bar{u}_n$	$\mathbf{T}^c\mathbf{\Psi}^c$	$(\mathbf{\Psi}^m\mathbf{T}^m)\bar{u}_n = 0$
	$\mathbf{T}^c\mathbf{\Psi}^c$ is determined by the location of control source	$(\mathbf{\Psi}^m\mathbf{T}^m)^H$ is determined by the location of error microphone

Substitution of equation (19) into equation (15) gives

$$W^t = \left(\sum_{n=1}^{N} c_n \bar{u}_n\right)^H (\mathbf{I} - \mathbf{C})^H \mathbf{A} (\mathbf{I} - \mathbf{C}) \left(\sum_{n=1}^{N} c_n \bar{u}_n\right). \tag{20}$$

From equations (17), (18), and (19), one can see that

$$(\mathbf{I} - \mathbf{C}) \sum_{n=1}^{N} c_n \bar{u}_n = \sum_{n=2}^{N} c_n \bar{u}_n .$$

Thus, equation (20) can be written in a simplified form as

$$W^t = \left(\sum_{n=2}^{N} c_n \bar{u}_n\right)^H \mathbf{A} \left(\sum_{n=2}^{N} c_n \bar{u}_n\right). \tag{21}$$

In equation (21), one can observe that the $\bar{u}_1$ component of $\overline{\beta}$ is controlled by the control system, but the $\bar{u}_2 \sim \bar{u}_N$ components of $\overline{\beta}$ are uncontrolled. This is because the error microphone cannot measure the $\bar{u}_2 \sim \bar{u}_N$ component of $\overline{\beta}$ ($\mathbf{\Psi}^m \mathbf{T}^m \bar{u}_n = 0$, $(n = 2 \sim N)$). It is noteworthy that the control performance of the control system, which consists of fewer sensors and actuators than N, depends on the primary sound field. One can deduce that for $\overline{\beta}$, whose direction coincides with that of $\bar{u}_1$, the control system can completely reduce the radiation power. In addition, the smaller the difference between the direction of $\overline{\beta}$ and $\bar{u}_1$, the smaller the residual radiation power will be. It is noteworthy that $\overline{\beta}$ has uncertainty since only parts of $\bar{u}_n$'s are assumed to be measured. Then, the next question is what is the degree of success in reducing the radiation power under this uncertain circumstance. The issues associated with this question are dealt with next.

4. ROBUST RELIABILITY OF THE CONTROL SYSTEM

This section addresses the robust reliability [3] of the control system. For this purpose, a set of primary sound fields, which can be produced at duct termination, will be defined. The robust reliability of the control system which has fewer sensors and actuators than N, and the condition for implementing the robust radiation power control system will be discussed.

4.1. THE SET OF PRIMARY SOUND FIELDS

As discussed in section 3.2, the performance of the control system, which consists of a smaller number of sensors and actuators than N, depends on the primary sound field variables ($\overline{\beta}$). It is desired to have the residual radiation power after the control to be less than that of the uncontrolled value, regardless of what primary sound field actually occurs in practice. One may say that such a control system is robust with respect to the uncertainty in the primary sound field. For the practical implementation of the control system, it is necessary to study the robust reliability [3] of such a control system.

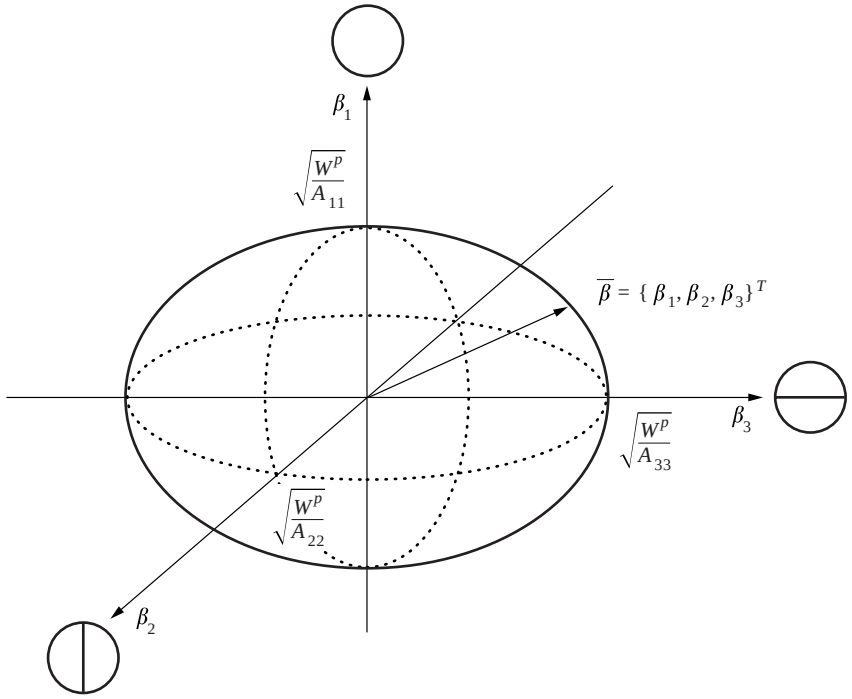

Figure 4. Example of a set of sound field variables $S(W^p)$ $(N = 3)$.

The first thing one has to do is to have a model that can appropriately express the noise source which has uncertainty. From equation (15), the radiation power due to arbitrary primary sources can be represented as

$$W^p = \overline{\beta}^H \mathbf{A} \overline{\beta}. \tag{22}$$

If one does not have any information about the primary sources, then the control problem has to deal with the uncertainty associated with primary sources. Therefore, our main interest is to find a control strategy when we do not know $\overline{\beta}$, this results in uncertainty in $\overline{\beta}$.

This uncertainty can be written by using the uncertainty principle [3]. The set of functions $(p^p(r, \theta, 0))$ for which the coefficients $(\overline{\beta})$ lie on the surface of an ellipsoid is defined as

$$S(W^p) = \{p^p(r, \theta, 0) = \overline{\psi}\overline{\beta} \mid \overline{\beta}^H \mathbf{A} \overline{\beta} = W^p\}, \tag{23}$$

where W^p is the radiation power produced due to the unknown primary sources (Figure 4). It is noteworthy that unknown variations of the primary sound field are represented by $S(W^p)$. In other words, $S(W^p)$ represents the set of all primary sound fields, which can be produced at duct termination, whose radiation powers are W^p. Each particular realization of the primary sound field, $p^p(r, \theta, 0)$, corresponds to a particular choice of $\overline{\beta}$ on the surface of the ellipsoid.

4.2. ROBUST RELIABILITY AND ROBUST RADIATION POWER CONTROL SYSTEM

The greatest possible residual radiation power, after applying the control system, can be expressed as

$$\hat{W}^t = \max_{\overline{\beta} \in S(W^p)} W^t. \tag{24}$$

If one defines $(\mathbf{I} - \mathbf{C})^H \mathbf{A}(\mathbf{I} - \mathbf{C})$ of equation (15) as $\mathbf{V}$, then equation (24) can be expressed as the following optimization problem.

$$\hat{W}^t = \max \overline{\beta}^H \mathbf{V} \overline{\beta}, \quad \text{constraint} \quad \overline{\beta}^H \mathbf{A} \overline{\beta} = W^p. \tag{25}$$

The solution of this optimization problem is an eigenvalue problem [3]. One can find that the greatest possible residual radiation power ($\hat{W}^t$) is proportional to the greatest eigenvalue of a particular known matrix $\mathbf{A}^{-1/2H} \mathbf{V} \mathbf{A}^{-1/2}$ and W^p (see Appendix).

$$\hat{W}^t = \lambda_{max} W^p. \tag{26}$$

where λ_{max} is the greatest eigenvalue of the matrix $\mathbf{A}^{-1/2H} \mathbf{V} \mathbf{A}^{-1/2}$. Let $\bar{e}_{max}$ denote the normalized eigenvector corresponding to λ_{max}, then the direction of $\bar{e}_{max}$ coincides with that of $\mathbf{A}^{1/2} \overline{\beta}$, into which maximum radiation power ($\hat{W}^t$) occurs. It is noteworthy that when $\lambda_{max} \leqslant 1$, W^t is always less than W^p, regardless of the primary sound field. On the other hand, when $\lambda_{max} > 1$, the residual radiation power W^t would be larger than W^p for some $\overline{\beta}$ in $S(W^p)$. Equation (26) is the basic design equation for the robust control system since it shows us that one must design the control system to minimize λ_{max}. It should also be mentioned that λ_{max} is a measure of the robust reliability which accounts for the design of the control system and the uncertainty in the primary sound field.

Table 3 summarizes the eigenvalues λ_n and normalized eigenvectors ($\bar{e}_n$) of the matrix $\mathbf{A}^{-1/2H} \mathbf{V} \mathbf{A}^{-1/2}$ when $K = L = 1$. In Table 3, one can see that λ_{max} can be expressed as a function of $\bar{e}_1$ and $\bar{e}^m$,

$$\lambda_{max} = \left| \frac{1}{\bar{e}_1^H \bar{e}^m} \right|^2, \tag{27}$$

where $\bar{e}_1 = \mathbf{A}^{1/2} \mathbf{T}^c \mathbf{\Psi}^c / |\mathbf{A}^{1/2} \mathbf{T}^c \mathbf{\Psi}^c|$ is a function of the location of the control source, and $\bar{e}^m = (\mathbf{\Psi}^{m\prime} \mathbf{T}^m \mathbf{A}^{-1/2}) / |(\mathbf{\Psi}^{m\prime} \mathbf{T}^m \mathbf{A}^{-1/2})|$ is a function of the location of the error microphone. Physically, $\bar{e}_1$ represents the direction of $\mathbf{A}^{1/2} \overline{\beta}$ for minimum radiation power occurrence. $\bar{e}^m$ represents the vector that is orthogonal to the unobservable plane (Figure 5).

From equation (27), one can observe that as the difference between the direction of $\bar{e}_1$ and $\bar{e}^m$ increases, λ_{max} increases. It is noteworthy that the minimum value of λ_{max} is 1, and it occurs when the direction of $\bar{e}_1$ coincides with that of $\bar{e}^m$. Therefore, one can see that for the robust control of the radiation power ($W^t \leqslant W^p$) for any $\overline{\beta}$ in $S(W^p)$, one has to design a control system that satisfies the following condition, such that

$$\mathbf{A} \mathbf{T}^e \mathbf{\Psi}^c = \alpha (\mathbf{\Psi}^{m\prime} \mathbf{T}^m)^H, \tag{28}$$

TABLE 3

Eigenvalues (λ_n) *and normalized eigenvectors* ($\bar{e}_n$) *of* $\mathbf{A}^{-1/2H}\mathbf{V}\mathbf{A}^{-1/2}$ ($K = L = 1$)

n	1	$2 \sim N-1$	N
λ_n	0	1	$\left\lvert \frac{1}{\bar{e}_1^H \bar{e}^m} \right\rvert^2$
$\bar{e}_n$	$\frac{\mathbf{A}^{1/2}\mathbf{T}^e\mathbf{\Psi}^c}{\lvert\mathbf{A}^{1/2}\mathbf{T}^e\mathbf{\Psi}^c\rvert}$	$\bar{e}^{mH}\bar{e}_n = 0$	$\bar{e}_n^H \bar{e}_N = 0$
		$\bar{e}_1^H \bar{e}_n = 0$	$(N = 1 \sim N-1)$
		$\bar{e}_N^H \bar{e}_n = 0$	
	$\bar{e}_1$ represents the direction of $\mathbf{A}^{1/2}\overline{\beta}$ which is perfectly controllable	$\bar{e}_n$ represents the direction of $\mathbf{A}^{1/2}\overline{\beta}$ which is unobservable and uncontrollable	$\bar{e}_N$ represents the direction of $\mathbf{A}^{1/2}\overline{\beta}$ which is observable but uncontrollable

$\bar{e}^m = (\mathbf{\Psi}^{mr}\mathbf{T}^m\mathbf{A}^{-1/2})^H / \lvert(\mathbf{\Psi}^{mr}\mathbf{T}^m\mathbf{A}^{-1/2})^H\rvert$.

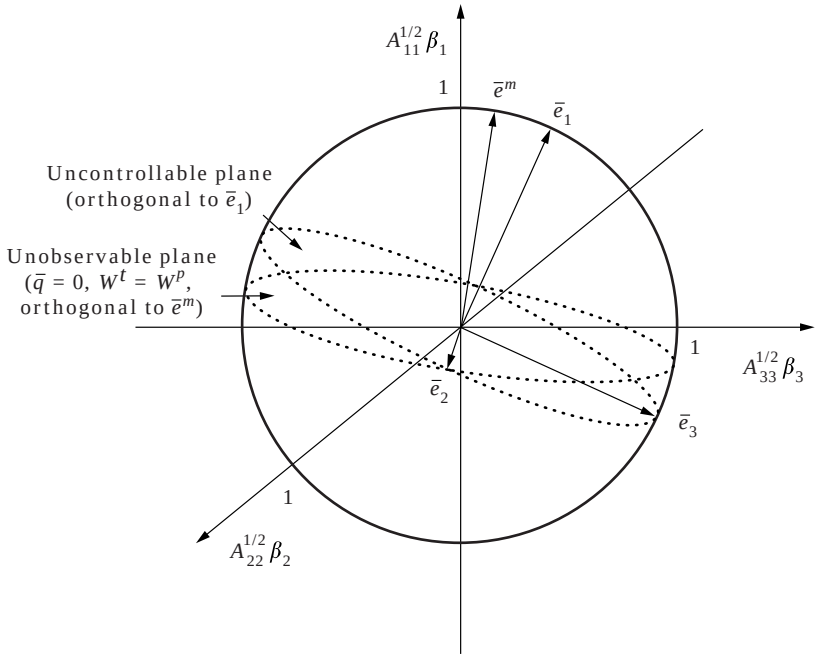

Figure 5. Example of normalized eigenvectors $\bar{e}_n$ of matrix $\mathbf{A}^{-1/2H}\mathbf{V}\mathbf{A}^{-1/2}$, and $\bar{e}^m$ ($K = L = 1$, $N = 3$; see Table 3).

where α is a complex constant. Physically, equation (28) means that the error microphone does not measure the uncontrollable component for the control source located at $\mathbf{x}_1^c$; it only measures the controllable component for the control source (Figure 5).

5. NUMERICAL SIMULATIONS AND EXPERIMENTS

For the verification of the theoretical analysis results obtained in sections 3 and 4, numerical simulations and experiments are performed.

5.1. DESIGN OF THE ROBUST RADIATION POWER CONTROL SYSTEM

Based on theoretical analysis, a control system, which satisfies equation (28), is designed. The control system has one error microphone and one control source to reduce the radiation power consisting of the three propagating modes (Table 1).

For the case of $N = 3$, $K = L = 1$, $\mathbf{A}\mathbf{T}^c\mathbf{\Psi}^c$ and $(\mathbf{\Psi}^m\mathbf{T}^m)^H$ in equation (28) can be expressed as

$$\mathbf{A}\mathbf{T}^c\mathbf{\Psi}^c = A_{11}T_{11}^c\left\{1, \frac{A_{22}T_{22}^c}{A_{11}T_{11}^c}N_2J_1(k_{r2}r_1^c)\cos\theta_1^c, \frac{A_{33}T_{33}^c}{A_{11}T_{11}^c}N_3J_1(k_{r3}r_1^c)\sin\theta_1^c\right\}^T, \quad (29)$$

$$(\mathbf{\Psi}^m\mathbf{T}^m)^H = T_{11}^{m*}\left\{1, \frac{T_{22}^{m*}}{T_{11}^{m*}}N_2J_1(k_{r2}r_1^m)\cos\theta_1^m, \frac{T_{33}^{m*}}{T_{11}^{m*}}N_3J_1(k_{r3}r_1^m)\sin\theta_1^m\right\}^T, \quad (30)$$

where N_2 and N_3 are the normalization factors of the eigenfunction, k_{rn} is the wave number in r direction, and $J_1(\cdot)$ is the Bessel function of the first kind of order 1. Since $R_2 = R_3$ and $k_{r2} = k_{r3}$ (Table 1), one can see that

$$\frac{A_{33}T_{33}^c}{A_{11}T_{11}^c} = \frac{A_{22}T_{22}^c}{A_{11}T_{11}^c} \quad \text{and} \quad \frac{T_{33}^{m*}}{T_{11}^{m*}} = \frac{T_{22}^{m*}}{T_{11}^{m*}}.$$

From equations (28), (29), and (30), the condition for the robust control system can be expressed as

$$\frac{A_{22}T_{22}^c}{A_{11}T_{11}^c} J_1(k_{r2}r_1^c) = \frac{T_{22}^{m*}}{T_{11}^{m*}} J_1(k_{r2}r_1^m), \qquad \theta_1^c = \theta_1^m. \tag{31a, b}$$

For example, if the frequency of the primary source is 460 Hz, and if one selects the position of the control source at $\mathbf{x}_1^c = (0{\cdot}5r_0,\ 0\ \pi,\ -1{\cdot}3m)$, then several error microphone locations, which satisfy equation (31), can be obtained. One of those possible microphone locations is $\mathbf{x}_1^m = (0{\cdot}28r_0,\ 0\ \pi,\ -0{\cdot}15m)$. The schematic diagram of this control system is shown in Figure 6. The following describes the control performance and robust reliability of this control system.

5.2. THE RESULTS OF NUMERICAL SIMULATION

The numerical simulation gives that λ_{max} of the control system (Figure 6) is 1. The eigenvector ($\bar{e}_{max}$), which represents the direction of $\mathbf{A}^{1/2}\overline{\beta}$ for maximum residual radiation power ($\hat{W}^r$) occurrence is found to be $\{0{\cdot}827,\ -0{\cdot}495 - j0{\cdot}269,\ 0\}^T$. Similarly, the eigenvector ($\bar{e}_1$) representing the direction of $\mathbf{A}^{1/2}\overline{\beta}$ for minimum residual radiation power occurrence is found to be $\{0{\cdot}495 - j0{\cdot}269,\ 0{\cdot}827,\ 0\}^T$ (Table 3).

Figure 7 represents the control performance of this control system. Figure 7(a) is a plot of the pressure field at $z = z^m$, when $\mathbf{A}^{1/2}\overline{\beta}$ coincides with $\bar{e}_1$. In Figure 7(a),

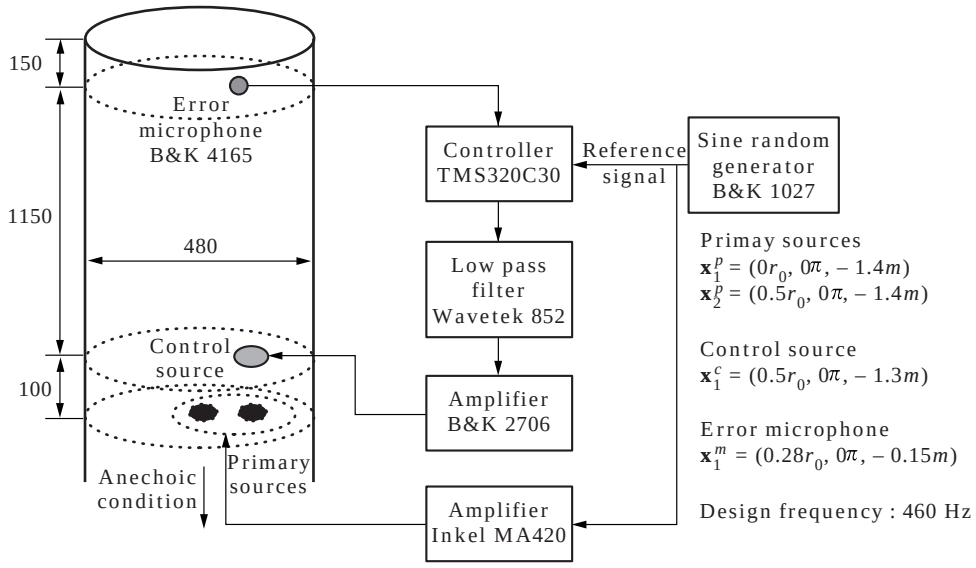

Figure 6. Schematic diagram of the experimental set-up for radiation power control (unit: mm).

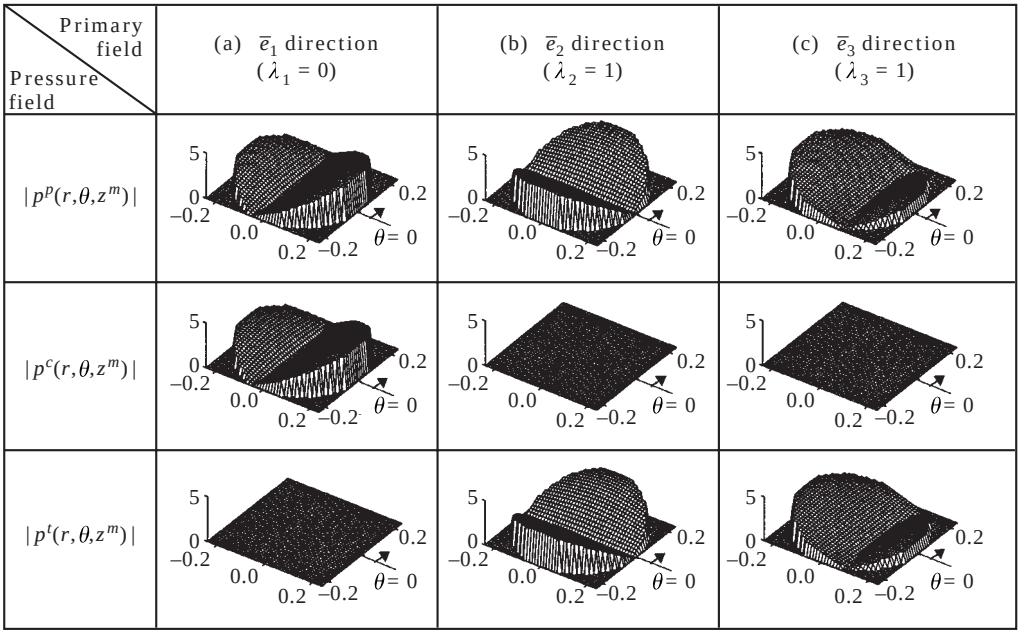

Figure 7. Control performance of the robust radiation power control system (frequency: 460 Hz, $\mathbf{x}_1^c = (0{\cdot}5r_0,\ 0\pi,\ -1{\cdot}3m)$, $\mathbf{x}_1^m = (0{\cdot}28r_0,\ 0\pi,\ -0{\cdot}15m)$, $r_0 = 0{\cdot}24$ m, $\bar{e}^m = \{0{\cdot}495 - j0{\cdot}269,\ 0{\cdot}827,\ 0\}^T$). (a) When $\mathbf{A}^{1/2}\overline{\beta} = \bar{e}_1 = \{0{\cdot}495 - j0{\cdot}269,\ 0{\cdot}827,\ 0\}^T$; (b) when $\mathbf{A}^{1/2}\overline{\beta} = \bar{e}_2 = \{0,\ 0,\ 1\}^T$; (c) when $\mathbf{A}^{1/2}\overline{\beta} = \bar{e}_{max} = \{0{\cdot}827,\ -0{\cdot}495 - j0{\cdot}269,\ 0\}^T$.

one can see that the control system can completely reduce the radiation power. Therefore, one can deduce that the smaller the difference between the direction of $\mathbf{A}^{1/2}\overline{\beta}$ and $\bar{e}_1$, the smaller the residual radiation power will be. Figure 7(b) represents the pressure field at $z = z^m$, when $\mathbf{A}^{1/2}\overline{\beta}$ coincides with $\bar{e}_2$. One can observe that $\mathbf{A}^{1/2}\overline{\beta}$, coinciding with $\bar{e}_2$, is unobservable and uncontrollable since $\bar{e}^{mH}\bar{e}_2 = 0$ and $\bar{e}_1^H\bar{e}_2 = 0$ (Table 3, Figure 5). Figure 7(c) represents the pressure field at $z = z^m$, when $\mathbf{A}^{1/2}\overline{\beta}$ coincides with $\bar{e}_{max}$. In Figure 7(c), one can observe that the pressure at the error microphone location ($\mathbf{x}_1^m = (0{\cdot}28r_0,\ 0\pi,\ -0{\cdot}15m)$) is 0, and the control system does not operate. This is because the error microphone does not measure the uncontrollable $\mathbf{A}^{1/2}\overline{\beta}$ for the control source located at $\mathbf{x}_1^c$. Since $\hat{W}^t = W^p$, one

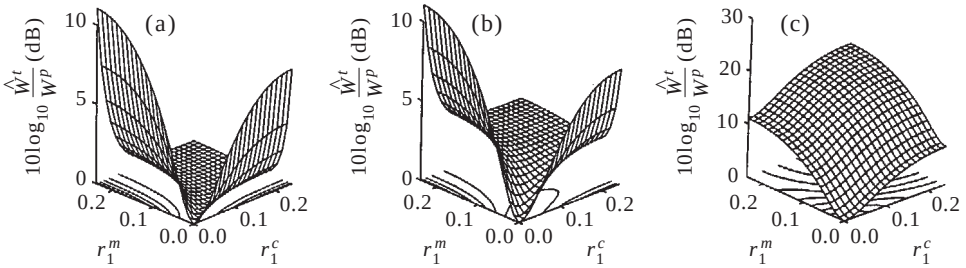

Figure 8. Robust reliability of the control system as a function of the locations of error microphone and control source (frequency: 460 Hz, $z^c = -1{\cdot}3m$, $z^m = -0{\cdot}15m$, $r_0 = 0{\cdot}24m$). (a) $\hat{W}^t/W^p(\theta_1^m = 0\pi,\ \theta_1^c = 0\pi)$; (b) $\hat{W}^t/W^p(\theta_1^m = 0{\cdot}125\pi,\ \theta_1^c = 0\pi)$; (c) $\hat{W}^t/W^p(\theta_1^m = 0{\cdot}25\pi,\ \theta_1^c = 0\pi)$.

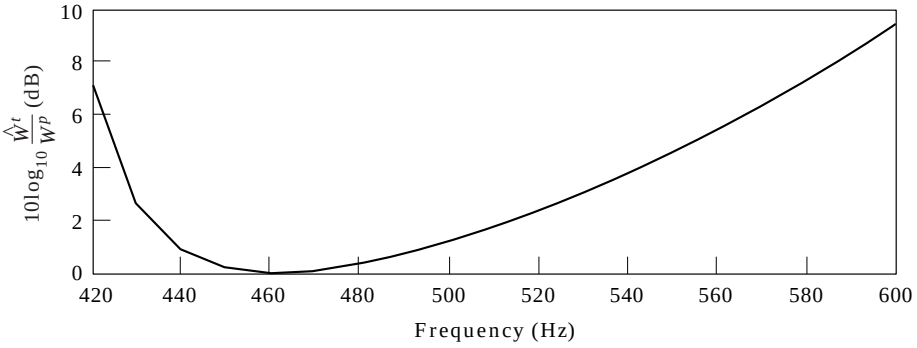

Figure 9. Robust reliability of the control system as frequency varies ($\mathbf{x}_1^c = (0{\cdot}5r_0,\ 0\pi,\ -1{\cdot}3m)$, $\mathbf{x}_1^m = 0{\cdot}28r_0,\ 0\pi,\ -0{\cdot}15m)$, $r_0 = 0{\cdot}24m$).

can verify that this control system is robust with respect to the uncertainty in the primary sound field.

As mentioned in section 4.2, λ_{max} is a measure of the robust reliability which accounts for the design of the control system and the uncertainty in the primary sound field. For comparison of the robust reliability of the control system, which satisfies equation (31), with other non-robust control systems, λ_{max} is calculated in terms of the locations of error microphone and control source. Figure 8 is the plot of $\hat{W}^t/W^p(=\lambda_{max})$ on the decibel scale when the locations of error microphone and control source vary. In Figure 8, one can see that the control systems, which satisfy equation (31), are robust with respect to the uncertainty in the primary sound field ($\hat{W}^t = W^p$). On the other hand, for the cases that do not satisfy equation (31), one can observe that $\hat{W}^t/W^p$ is larger than 1, and the control system is not robust ($\hat{W}^t > W^p$), as typically demonstrated in Figures 8(b) and (c).

Since $A_{22}T_{22}^c/A_{11}T_{11}^c$ and T_{22}^{m*}/T_{11}^{m*} in equation (31) are the functions of frequency, it is necessary to investigate the robust reliability of the control system in terms of frequency. Figure 9 shows the robust reliability of the control system (Figure 6) as frequency varies. In Figure 9, one can see that as the difference between the primary source frequency and the design frequency (460 Hz) increases, the magnitude of $\hat{W}^t/W^p$ increases, and the control system is no longer robust. On the other hand, in the narrow frequency band centered at the design frequency (406 Hz), one can see that $\hat{W}^t/W^p$ is nearly 1, and the control system has robust control performance. Thus, one can deduce that the control system, which consists of fewer control sources and sensors than N, can be used for reducing the narrow frequency band noise centered at the design frequency.

5.3. EXPERIMENTAL RESULTS

Figure 6 is the schematic diagram of the experimental set-up. The active control experiment is conducted by implementing the time-domain filtered-x LMS adaptive algorithm [9, 10]. By using the generator signal as a reference input to the adaptive controller, the acoustic feedback problem is eliminated in the experiment.

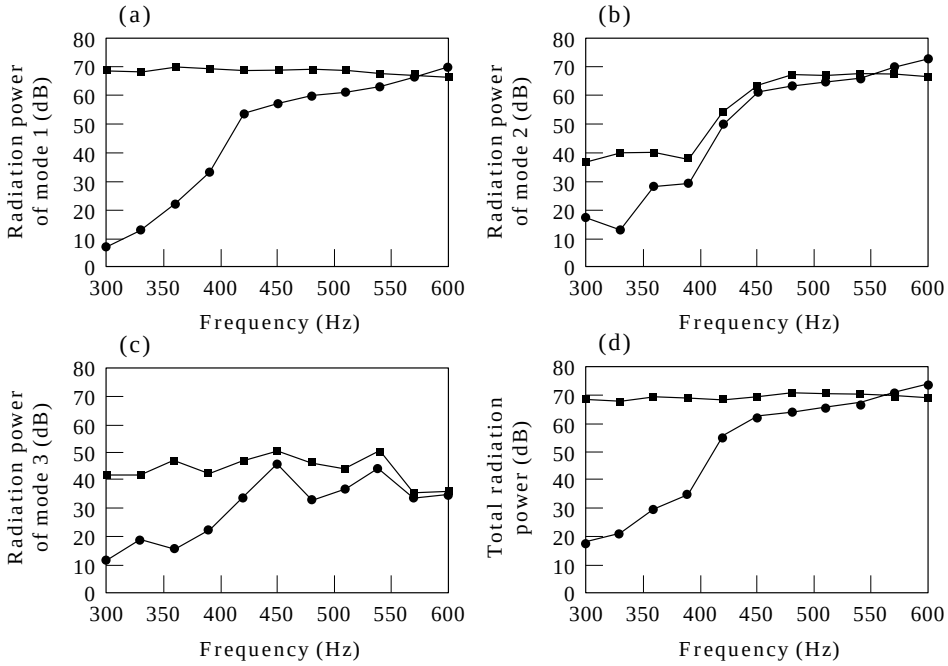

Figure 10. Control performance of the active control system when two primary sources at $\mathbf{x}_1^p = (0r_0, 0\pi, -1{\cdot}4m)$, $\mathbf{x}_2^p = (0{\cdot}5r_0, 0\pi, -1{\cdot}4m)$ are operated with equal volume velocity ($r_0 = 0{\cdot}24m$, $\mathbf{x}_1^c = (0{\cdot}5r_0, 0\pi, -1{\cdot}3m)$, $\mathbf{x}_1^m = (0{\cdot}28r_0, 0\pi, -0{\cdot}15m)$). Radiation power of (a) mode 1, (b) mode 2, (c) mode 3, (d) total radiation power. —■—, Before control; —●—, after control.

First, control performance is investigated in terms of sound field variables. For the generation of primary sound fields that consist of two modes ($\psi_1(r, \theta), \psi_2(r, \theta)$), two primary sources located at $\mathbf{x}_1^p = (0r_0, 0\pi, -1{\cdot}4m)$ and $\mathbf{x}_2^p = (0{\cdot}5r_0, 0\pi, -1{\cdot}4m)$ are used.

Figure 10 is the experimental result when two primary sources at $\mathbf{x}_1^p$, $\mathbf{x}_2^p$ are operated with equal volume velocity. Figures 10(a)–(c) show radiation power of the first, second, and third modes respectively. Figure 10(d) shows total radiation

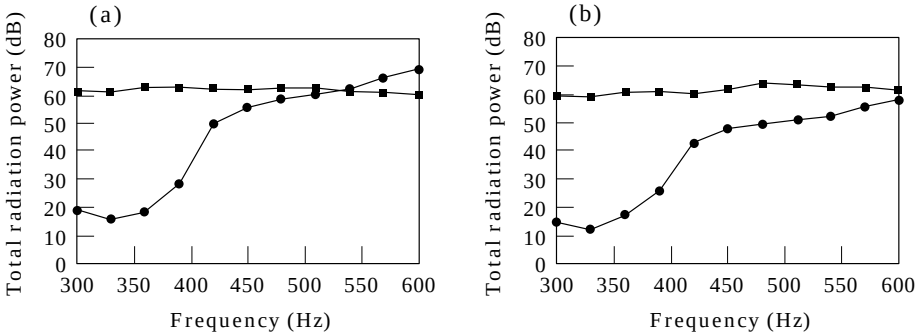

Figure 11. Control performance of the active control system with varying primary sound field ($r_0 = 0{\cdot}24m$, $\mathbf{x}_1^c = (0{\cdot}5r_0, 0\pi, -1{\cdot}3m)$, $\mathbf{x}_1^m = (0{\cdot}28r_0, 0\pi, -0{\cdot}15m)$). (a) Total radiation power when the primary source at $\mathbf{x}_1^p = (0r_0, 0\pi, -1{\cdot}4m)$ is operated; (b) total radiation power when the primary source at $\mathbf{x}_2^p = (0{\cdot}5r_0, 0\pi, -1{\cdot}4m)$ is operated. Key as for Figure 10.

power at duct termination. In Figure 10(d), above the first cut-off frequency (419 Hz), one can see that it is possible to reduce the radiation power, which consists of higher modes, by using only one error microphone and one control source. It also shows that the control performance of the control system slowly degrades and increases the radiation power above 550 Hz. This is because equation (31) is not satisfied at that frequency region since the locations of control source and sensor are designed for 460 Hz (Figure 9). Thus, one can deduce that a control system with fewer control sources and sensors than N could be used for the reduction of the narrow frequency band noise centered at the design frequency.

Figure 11(a) shows the total radiation power when the primary source at $\mathbf{x}_1^p = (0r_0, 0\pi, -1{\cdot}4m)$ is operated. Figure 11(b) is the experimental result when the primary source located at $\mathbf{x}_2^p = (0{\cdot}5r_0, 0\pi, -1{\cdot}4m)$ is operated.

By comparing Figure 11(a) with Figure 10(d), one can see that the control performance of Figure 11(a) is worse than that of Figure 10(d) since the difference between the direction of $\mathbf{A}^{1/2}\overline{\beta}$ and $\bar{e}_1$ of Figure 11(a) is larger than that of Figure 10(d) (Table 3 and Figure 5). On the other hand, Figure 11(b) shows better control performance than Figure 10(d) since the difference between the direction of $\mathbf{A}^{1/2}\overline{\beta}$ and $\bar{e}_1$ of Figure 11(b) is smaller than that of Figure 10(d).

It should also be mentioned that in the low frequency region below the first cut-off frequency (419 Hz), irrespective of the locations of the primary sources, relatively good control performance is accomplished, as shown in Figure 10(d), 11(a) and 11(b). The reason for such good control performance lies in the fact that only planewave is propagated below the cut-off frequency.

For comparison of the control performance of the robust control system with the other non-robust control systems, the radiation power reduction of these control systems are measured experimentally. Table 4 summarizes the experimental results performed at the design frequency (460 Hz). Table 4 shows the control performances of the robust control system (case (1)) and the other systems (cases (2)–(8)) whose error microphone is located at non-optimum

TABLE 4

Radiation power reductions (dB) of the robust control system and non-robust control systems ($\mathbf{x}_1^p = (0r_0, 0\pi, -1{\cdot}4m)$, $\mathbf{x}_2^p = (0{\cdot}5r_0, 0\pi, -1{\cdot}4m)$, $\mathbf{x}_1^c = (0{\cdot}5r_0, 0\pi, -1{\cdot}3m)$, *frequency* = 460 *Hz*)

Location of error microphone	Primary sources at $\mathbf{x}_1^p$, $\mathbf{x}_2^p$ are operated with equal volume velocity	Primary source at $\mathbf{x}_1^p$ is operated	Primary source at $\mathbf{x}_1^p$ is operated
(1) $\mathbf{x}_1^m = (0{\cdot}28r_0, 0\pi, -0{\cdot}15m$	9·3	5·2	12·3
(2) $\mathbf{x}_1^m = (0r_0, 0\pi, -0{\cdot}15m$	7·2	2·0	10·8
(3) $\mathbf{x}_1^m = (0{\cdot}5r_0, 0\pi, -0{\cdot}15m$	7·8	3·7	10·7
(4) $\mathbf{x}_1^m = (1{\cdot}0r_0, 0\pi, -0{\cdot}15m$	7·0	2·7	10·0
(5) $\mathbf{x}_1^m = (0{\cdot}5r_0, 0{\cdot}5\pi, -0{\cdot}15m$	5·2	1·6	7·1
(6) $\mathbf{x}_1^m = (1{\cdot}0r_0, 0—5\pi, -0{\cdot}15m$	2·5	0·3	4·2
(7) $\mathbf{x}_1^m = (0{\cdot}5r_0, \pi, -0{\cdot}15m$	−2·4	−5·0	1·8
(8) $\mathbf{x}_1^m = (1{\cdot}0r_0, \pi, -0{\cdot}15m$	−9·3	−4·2	3·5

positions for robust control. In Table 4, one can observe that the robust control system (case (1)) performs the best, as expected. In other cases, the power reductions that can be obtained are less than that of case (1)). It should also be mentioned that the radiation power reductions are negative (W^r is larger than W^p) for some primary sound fields since these control systems do not satisfy equation (31).

From the experimental results one can confirm that it is possible to control the radiation power, which consists of higher modes in the narrow frequency band centered at the design frequency, by using one error microphone and one control source appropriately placed. It should also be mentioned that the control performance of the robust control system (case (1)) is better than the non-robust control systems (cases (2)–(8)) that do not satisfy equation (31).

6. CONCLUSIONS

A study on the control performance and robust reliability of an active control system, which has fewer sensors and actuators than the number of propagating modes in a duct, has been carried out.

The equations of residual radiation power at duct termination were derived as a function of sound field variables and control systems variables. Then, by theoretical analysis and numerical simulation, the control performance and robust reliability of the control system were investigated in terms of sound field variables and control system variables. The control system, which has one error microphone and one control source for reducing radiation power consisting of three propagating modes, was considered for its simplicity. The possibility of implementing the robust radiation power control system was also verified by theoretical analysis and numerical simulation.

ACKNOWLEDGMENT

This work is supported by Hyundai Marine Research Institute. The authors acknowledge the help and participation of the Noise and Vibration of HMRI for the completion of this research.

REFERENCES

1. I.-S. Kim and K.-J. Kim 1994 *Mechanical System and Signal Processing* **8**, 93–108. Active control of cross mode waves in rectangular ducts.
2. T. Morishita, C. Yamaguchi, T. Tanaka and M. Taki 1994 *Proceedings of Inter-Noise* 94, *Yokohama*, *Japan*, 1373–1376. Active control of noise including higher-order acoustic modes propagating in a duct.
3. Yakov Ben-Haim 1996 *Robust Reliability in the Mechanical Sciences*. Berlin: Springer. See Chapter 3.
4. M. L. Munjal 1987 *Acoustics of Ducts and Mufflers*. New York: Wiley. See pp. 9–12.

5. P. E. Doak 1973 *Journal of Sound and Vibration* **31**, 1–72. Excitation, transmission and radiation of sound from source distribution in hard-walled ducts of finite length (I): the effects of duct cross-section geometry and source distribution space-time pattern.
6. P. E. Doak 1973 *Journal of Sound and Vibration* **31**, 137–174. Excitation, transmission and radiation of sound from source distribution in hard-walled ducts of finite length (II): the effects of duct length.
7. S. W. Kang and Yang-Hann Kim 1995 *Journal of Sound and Vibration* **181**, 765–780. Green function analysis of the acoustic field in a finite three-port circular chamber.
8. P. Lancaster and M. Tismenetsky 1985 *The Theory of Matrices with Applications*. London: Academic Press; second edition. See pp. 432–440.
9. P. A. Nelson and S. J. Elliott 1992 *Active Control of Sound*. London: Academic Press. See pp. 195–198.
10. B. Widrow and S. D. Sterns 1985 *Adaptive Signal Processing*. Englewood Cliffs, NJ: Prentice-Hall. See pp. 288–292.

APPENDIX: GREATEST POSSIBLE RESIDUAL RADIATION POWER

The residual radiation power (W^t) for arbitrary $\overline{\beta}$ in $S(W^p)$ can be expressed as

$$W^t = \overline{\beta}^H \mathbf{V} \overline{\beta} + \lambda (W^p - \overline{\beta}^H \mathbf{A} \overline{\beta}), \tag{A1}$$

where λ is the Lagrange multiplier for the equality constraint, $\overline{\beta}^H \mathbf{A} \overline{\beta} = W^p$.

Differentiation of W^t, with respect to $\overline{\beta}$ and λ, yields necessary conditions for an extremum as

$$\frac{\partial W^t}{\partial \overline{\beta}} = \mathbf{V} \overline{\beta} - \lambda \mathbf{A} \overline{\beta} = 0, \qquad \frac{\partial W^t}{\partial \lambda} = W^p - \overline{\beta}^H \mathbf{A} \overline{\beta} = 0. \tag{A2a, b}$$

Equations (A2) can be rewritten as

$$\mathbf{V} \overline{\beta} = \lambda \mathbf{A} \overline{\beta}, \qquad \overline{\beta}^H \mathbf{A} \overline{\beta} = W^p. \tag{A3a, b}$$

Let $\overline{\beta}' = \mathbf{A}^{1/2} \overline{\beta}$, then equations (A3) can be expressed as

$$\mathbf{A}^{-1/2H} \mathbf{V} \mathbf{A}^{-1/2} \overline{\beta}' = \lambda \overline{\beta}', \qquad \overline{\beta}'^H \overline{\beta}' = W^p. \tag{A4a, b}$$

Equations (A4) shows that λ must be the eigenvalue of $\mathbf{A}^{-1/2H} \mathbf{V} \mathbf{A}^{-1/2}$, and $\overline{\beta}'$ is the corresponding eigenvector.

Premultiplying both sides of equation (A4a) by $\overline{\beta}'^H$ gives

$$\overline{\beta}'^H \mathbf{A}^{-1/2H} \mathbf{V} \mathbf{A}^{-1/2} \overline{\beta}' = \lambda \overline{\beta}'^H \overline{\beta}'. \tag{A5}$$

From equation (A4b), equation (A5) can be expressed as

$$\overline{\beta}^H \mathbf{V} \overline{\beta} = \lambda W^p. \tag{A6}$$

To maximize W^t, λ should be the largest eigenvalue of $\mathbf{A}^{-1/2H} \mathbf{V} \mathbf{A}^{-1/2}$; therefore, the greatest possible residual radiation power, $\hat{W}^t$, can be expressed as

$$\hat{W}^t = \lambda_{max} W^p, \tag{A7}$$

where λ_{max} is the greatest eigenvalue of $\mathbf{A}^{-1/2H} \mathbf{V} \mathbf{A}^{-1/2}$.